Noorhana Yahya

ADVANCED STRUCTURED MATERIALS 5

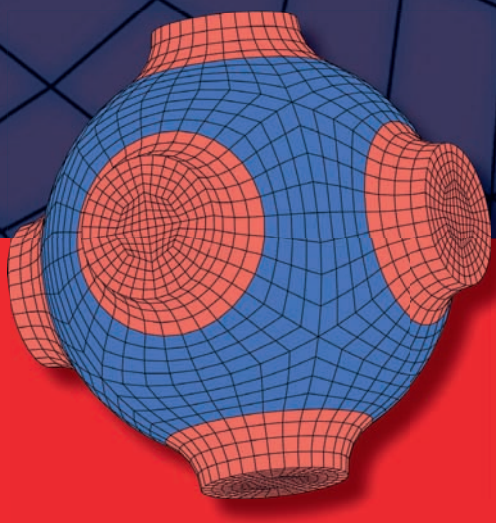

Carbon and Oxide Nanostructures

Synthesis, Characterisation and Applications

Springer

Advanced Structured Materials

Volume 5

For further volumes:
http://www.springer.com/series/8611

Noorhana Yahya

Carbon and Oxide Nanostructures

Synthesis, Characterisation and Applications

Springer

Assoc. Prof. Dr. Noorhana Yahya
Department of Fundamental and Applied Sciences
Universiti Teknologi PETRONAS
Bandar Seri Iskandar
31750 Tronoh, Perak
Malaysia
noorhana_yahya@petronas.com.my

ISSN 1869-8433
ISBN 978-3-642-14672-5 e-ISBN 978-3-642-14673-2
DOI 10.1007/978-3-642-14673-2
Springer Heidelberg Dordrecht London New York

Library of Congress Control Number: 2010937766

Cover design: WMXDesign GmbH, Heidelberg, Germany

Printed on acid-free paper

Springer is part of Springer Science+Business Media (www.springer.com)

Preface

It is my privilege as the Editor-in-Chief to present to you an effort of our team of prominent contributors to this monograph on Carbon and Oxide Nanostructures. Over the past 20 years, carbon and oxide nanostructures evolved into one of the most studied objects and are presently entering in the transition phase from nanoscience to nanotechnology. Carbon and oxide nanostructures constitute an enormous topic which may only be described in a simplified manner, which in essence is the intent of this book. It is hoped that this book would provide valuable resources for researchers as well as postgraduate students of physics, chemistry and engineering. Related carbon-based materials such as fullerenes, carbon fiber, glassy carbon, carbon black, amorphous carbon, diamond, graphite, buckminsterfullerene, and carbon nanotubes (CNTs) are discussed. CNTs which have attracted the attention of the scientific community due to their fundamental and technical importance are elaborated. It also presents a review of the applications of fullerene and its derivatives as electron beam resists, as well as outlining the effects of catalyst on the morphology of the carbon nanotubes. Structural and optical properties of hydrogenated amorphous carbon (a-C:H) thin films prepared in a DC-plasma-enhanced chemical vapor deposition reactor is discussed in greater detail. Some of the works done on polymer-CNTs-based solar cells with a variety of device architecture and band diagram are summarized. Several irregular configurations of carbon nanofibers (CNF) such as coiled, regular helical, and twisted coil are elaborated. This book also includes the molecular modeling of carbon-based nanomaterials including discussions on some aspects of the issues related to the synthesis and characterization of diamond prepared via CVD techniques using the hot filaments and plasma. Oxide-based materials related to fuel synthesis and solar hydrogen production are also presented. The versatility of ZnO nanostructures and some of the novel applications such as solar cells and light-emitting devices are being highlighted. A brief introduction of Fe–FeO nanocomposites and some superparamagnetism studies in the form of particles and thin films are included. The benefits and drawbacks of the properties of some nanomaterials used in optical sensing applications are given, and the recently developed optical chemical sensors and probes based on photoluminescence are also rigorously overviewed. Aspects of nanocatalytic reactions, the types of catalyst, and also the preparation and characterization of the active catalyst for ammonia synthesis are scrutinized.

I am grateful to all authors who have contributed to the chapters of this book. All merits on overview of such an enormous topic as Carbon and Oxide Nanostructures in this concise monograph should be credited to all contributing authors, but any shortcomings to be attributed to the Editor-in-Chief. The book is dedicated with all sincerity to all whose work has not received due reference and recognition.

Universiti Teknologi PETRONAS Assoc. Prof. Dr. Noorhana Yahya
Malaysia

Contents

Hydrogenated Amorphous Carbon Films

Suriani Abu Bakar, Azira Abdul Aziz, Putut Marwoto, Samsudi Sakrani, Roslan Md Nor, and Mohamad Rusop

Abstract Hydrogenated amorphous carbon (a-C:H) thin film is one of the most studied materials due to its unique features. The a-C:H thin film is a remarkable material because of its novel optical, mechanical and electrical properties and its similarities to diamond. In this chapter we reviewed the structural and optical properties of hydrogenated amorphous carbon (a-C:H) thin films prepared in a DC-PECVD reactor. Both power and ion bombardment energy were continuously changed during the deposition, as a results of varying deposition parameters such as

S.A. Bakar
Department of Physics, Faculty of Science and Technology, Universiti Pendidikan Sultan Idris, 35900 Tanjung Malim, Perak, Malaysia
e-mail: absuriani@yahoo.com

A.A. Aziz
NANO-SciTech Centre, Institute of Science, Universiti Teknologi MARA, 40450 Shah Alam, Selangor, Malaysia
e-mail: azira.aziz@gmail.com

P. Marwoto
Physics Department, Faculty of Mathematics and Science, Semarang State University, 50229, Semarang, Indonesia
e-mail: pmarwoto@yahoo.com

S. Sakrani
Physics Department, Faculty of Science, Universiti Teknologi Malaysia, 81310, Skudai, Johor, Malaysia
e-mail: samsudi@difz2.fs.utm.my

R. Md. Nor
Department of Physics, Faculty of Science, University of Malaya, 50603, Kuala Lumpur, Malaysia
e-mail: rmdnor@um.edu.my

M. Rusop
NANO-SciTech Centre, Institute of Science, Universiti Teknologi MARA, 40450 Shah Alam, Selangor, Malaysia
e-mail: rusop8@gmail.com

N. Yahya (ed.), *Carbon and Oxide Nanostructures,* Adv Struct Mater 5,
DOI 10.1007/8611_2010_15,
Published online: 27 June 2010

chamber pressure, electrode distance, CH_4 flow rate, and substrate temperature. The films properties ranged from polymer-like to graphite-like a-C:H films, as the power and ion energy increased. The structure and the optical properties of a-C:H films were analyzed by infrared and Raman spectroscopy, UV–Vis Spectrophotometer and photoluminescence. This is to extract the information on sp^3/sp^2 and hydrogen contents, optical gap, E_0 and photoluminescence properties of a-C:H films. The films were found to consist of sp^2 clusters of which the size increases with increasing power and ion bombardment energy during the deposition, resulting in lower hydrogen, sp^3 content, optical gap and photoluminescence response. The increased in hydrogen termination from the films at higher ion energies results in bigger cluster size and produced graphitic films.

1 Introduction

Thin films are solid materials of either metal, semiconductor or insulator, deposited onto substrates at film thickness in the range of 10–1,000 nm [1]. Beyond this range they are referred to as thick films. The term ultra thin film is used for films with thickness smaller than 100 nm. Its thickness creates characteristics such as physical, chemical and mechanical properties which is different compared to the original bulk material and this contribute to a new phenomena. Substrate is any kind of solid that can support the formation of thin film on it. It is usually a material that does not interact with the film. A clean and smooth surface of substrate is required in order to obtain good quality and homogeneous films. Nowadays, we can see thin films widely used in electronics, optoelectronic devices, optical application and surface engineering applications [2].

Thin films can be produced by utilizing several methods. Generally, the preparation of thin films can be classified into two methods; physical and chemical techniques [3]. Some examples of physical vapor deposition are vacuum evaporation and sputtering. Meanwhile there are a variety of the chemical vapor deposition processes such as plasma enhanced (assisted) chemical vapor deposition (PECVD, PACVD), low-pressure chemical vapor deposition (LPCVD) and etc. Thin film production can be either in the form of single crystal, polycrystalline or amorphous, this depends on several factors such as temperature, pressure and etc during the deposition process.

Hydrogenated amorphous carbon (a-C:H) thin films is one of the most studied material due to its unique features. The a-C:H thin films is remarkable material because of its novel optical, mechanical and electrical properties and its similarities to diamond [4–6]. The main properties of diamond material are low optical absorption in UV, visible and IR regions, high electrical resistivity and thermal conductivity, extremely hard, low coefficient of friction and etc. [7–9]. The a-C:H material is not as excellent in optical, mechanical and electrical material as a single

crystal diamond, but it is adequate for numerous applications such as protective coating in areas namely optical window, scratch resistant, magnetic storage disk, biomedical coating and low friction wear resistant coatings for moving part in tools [6, 10].

The a-C:H thin films, is one of the diamond-like carbon (DLC) form. Aisernberg and Chabot [11] were the first to produce diamond-like carbon by ion beam deposition techniques. Angus et al. [12] defined pure DLC composed of carbon and hydrogen into two categories; hydrogenated amorphous carbon (a-C:H) and amorphous carbon (a-C). The a-C:H films contains less than 10–60% hydrogen (incorporations of hydrogen in the film are important to obtain diamond-like properties). The a-C films contain less than 1% hydrogen.

There are several deposition methods for a-C:H thin films production. These deposition methods can be categorized into two; physical vapor deposition (PVD) and plasma enhanced chemical vapor deposition (PECVD). PVD involves the sputtering of carbon atom from a solid target by energetic gas species, normally argon (Ar) ions [1]. PECVD method is widely used to deposit a-C:H films with better quality films as compared to chemical vapor deposition (CVD) method. PECVD involves a chemical process which takes place in the vapor phase at the substrate surface. As a result the films were deposited onto the substrate. The deposition process was conducted in low pressure ambient in the vapor phase.

In the PECVD method, there are two types of plasma species that contributes to the film growth; the radicals, (chemically active neutral species) and ions that diffuse from the plasma and drift toward the substrate surface [10]. The deposition parameters strongly affect the plasma species and the ionic energies as well as densities at the substrate [13].The deposition of a-C:H films by PECVD occur at low substrate temperatures, in contrast to CVD. In the PECVD method the high substrate temperature is overcome by applying electric field in the reactant gases to produce a significant number of free radicals, ion and etc. Due to the relatively low temperature, PECVD is a low-cost process as well. The power supply used to create the discharge in PECVD include RF [13–15], microwave (MW) – RF PECVD [16], RF – pulse DC mode PECVD [17], DC saddle field glow discharge [10, 18], DC – RF PECVD [4–19], electron cyclotron resonance (ECR) – MW Plasma Chemical Vapor Deposition (ECR-MPCVD) [20], microwave electron cyclotron resonance (ECR) – RF discharge PECVD [21, 22] etc.

Other than that, the study of a-C:H is very important since the structure of a-C:H is hardly understood as it consists of both sp^3 and sp^2 hybridized carbon. Both σ and π bond in a-C:H is definitely the difficulties faced in the analysis of the structure of a-C:H. Although, large amount of research has been done on a-C:H and as a-C:H films are already used in many applications, much about its properties have not been clearly comprehended. Until now, the Robertson model [6] is the most referred and successfully model. According to this model, amorphous carbon consists of sp^2 clusters, which are embedded in sp^3 bonded matrix. Hence it is the sp^2 sites that

forms band edges and controls the optical properties while sp^3 sites controlled mechanical properties.

In this chapter, we review the structural and optical properties of a-C:H thin films obtained by direct current-plasma enhanced chemical vapor deposition (DC-PECVD) method. The a-C:H properties, are highly affected by experimental parameters such as chamber pressure, electrode distance, methane (CH_4) flow rate, substrate temperature and etc. By changing the deposition parameters of a-C:H films, one can expect to obtain different sp^3 and sp^2 bond distributions and different structures in the films because it involves the change in plasma power and ion bombardment energy. Hence, the change in the properties of these films can be suited to specific applications.

2 Method of Preparing a-C:H Thin Film

2.1 Direct Current-Plasma Enhanced Chemical Vapor Deposition System

The PECVD method a is well-known method for the deposition of a-C:H thin film. Among of them is DC-PECVD method other than of radio frequency (RF)-PECVD. The DC-PECVD system consists of a deposition chamber (plasma reactor), power supply and gas system.

2.1.1 Plasma Reactor

The plasma reactor is constructed from stainless steel which is cylindrical in shape, having diameter of 15.24 cm and 20 cm in height. It is equipped with access door for putting in the sample and taking it out and a view port to observe the process, which is taking place inside the reactor. There are also channels for gas supply, vacuuming, electrical feed through (for DC power supply and heater) and linear motion feed through. Both anode and cathode are constructed from steel plate. Anode having diameter of 6.8 cm and thickness of 0.5 cm is connected to the DC power supply as shown in Fig. 1. Cathode which has the same diameter and thickness with anode is placed on the heater. It is then connected to the direct current and grounded together with the reactor's chamber wall. The cathode's distance to the anode can be changed in order to produce optimum plasma (1.5–4.0 cm). The cathode also acts as the substrate holder, where as the a-C:H films that were deposited on a corning glass substrates was placed on the cathode. This system is also shielded to avoid discharge from occurring at areas outside both electrode and to confine the plasma so that it stay in area between the two electrodes.

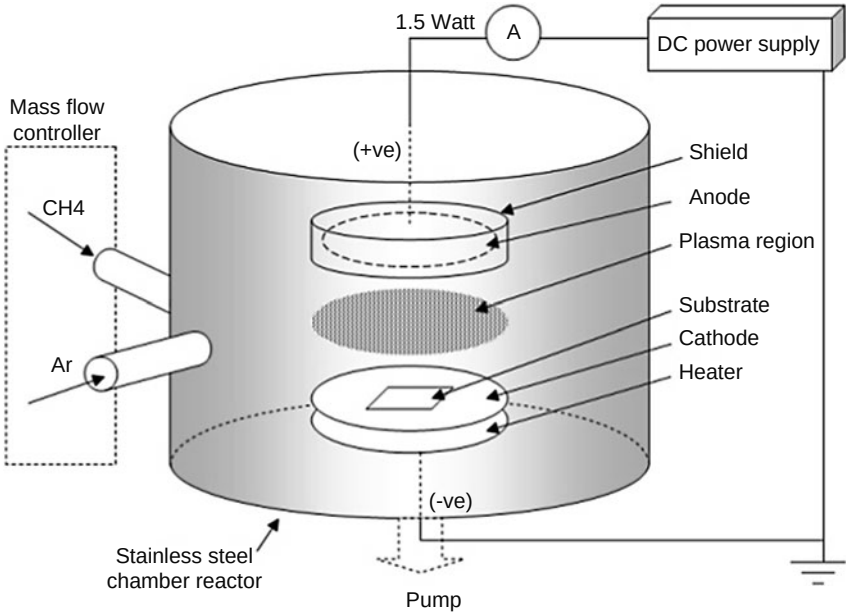

Fig. 1 DC-PECVD reactor schematic

2.1.2 Power Supply

Power supplies consist of two types:

1. Power supply for plasma formation
   The PECVD system used direct current power supply (DC). It provides 1.5 kV of voltage to produce maximum power of 1.5 W.
2. Power supply for heater
   The heater is capable of heating up the substrate at temperatures between 100 and 250°C.

2.1.3 Gas System

The gas systems consist:

1. The gases used: methane (CH_4), argon (Ar), and nitrogen (N_2).
2. Mass flow controller (MFC) used to measure and control the mass of gases that flow into the reactor chamber.
3. Vacuum system consists of vacuum pump (rotary mechanical pump), pressure gauge (Pirani gauge) and pressure controller. A vacuum of 10^{-2} Torr was achieved in the deposition chamber prior to the deposition.

This PECVD system is also equipped with an exhaust system in which all the unwanted gases from the reaction in the reactor will be ejected out using a pump via chimney.

3 Sample Preparation

In order to prepare the sample using DC-PECVD method, substrate was put on the substrate holder (cathode) within the reactor chamber with adjustable anode distance using linear motion feed trough. The entire samples were prepared in 5 hours (h). Before the deposition, substrates were cleaned with argon plasma with the following steps:

1. Reactor chamber were vacuumed to $\sim 2 \times 10^{-2}$ Torr.
2. Argon gas (3 sccm) was flowed into the reactor chamber.
3. Chamber pressure was maintained at 0.1 Torr using the variable valve.
4. DC power supply was turned on at 1.5 kV until Ar plasma was generated.
5. After 15 min, DC power supply was turned off.
6. The flow of Ar gas was stopped and the reactor chamber was vacuumed again.

After the cleaning process with Ar plasma was completed, the films deposition process was started. The deposition steps were as follows:

1. Reactor chamber were vacuumed to $\sim 2 \times 10^{-2}$ Torr.
2. Source gas (CH_4) with the desired rate was flowed into the reactor chamber (the operating deposition parameters were explained in the next section).
3. Chamber pressure was maintained at certain pressure.
4. DC power supply was turned on at 1.5 kV until plasma was generated.
5. After 5 h, DC power supply was turned off.
6. The flow of source gas was then stopped and the reactor chamber was vacuumed again to clean up all the gas residues within the chamber.
7. After the chamber pressure reaches $\sim 2 \times 10^{-2}$ Torr, the vacuumed pump was turn off.
8. Nitrogen gas was flowed into the reactor chamber until chamber pressure is equal to atmospheric pressure.
9. Take out the sample for structural and optical characterization.

4 Substrate Preparation

Prior to the growth process, the substrates were ultrasonically cleaned in order to achieve a good and uniform thin films deposition on the substrate surface.

The following procedure is followed:

1. A 30 min ultrasonic cleaned substrate in trichloroethylene.
2. Before continuing with acetone, methanol, the substrates were ultrasonic rinsed with deionized water (DI water).

3. A 30 min ultrasonic cleaned in acetone.
4. A 30 min ultrasonic cleaned in methanol.
5. And blow-dry the substrates using a hair dryer.
6. Put the substrates in a desiccator to avoid any contamination.

5 Deposition Parameters

Deposition parameters play an important role in the production of a-C:H films. Each parameter gives different effect to the a-C:H properties. Therefore optimization is required for excellent quality a-C:H. For a-C:H films which were deposited by DC-PECVD method the following parameter were experimented: chamber pressure, electrode distance, CH_4 flow rate and substrate temperature. Each set have five different samples.

The first set was deposited at chamber pressure between 0.1 and 0.8 Torr with all other parameter remain constant (Set 1) as shown in Table 1. The second set was deposited at electrode distances from 1.5 to 3.5 cm with all other parameter fixed (refer to Table 2). The next set was deposited by varying the CH_4 flow rate between 1 and 9 sccm (Set 3) as tabulated in Table 3. Finally, Set 4 was deposited by increasing the substrate temperature between 30 and 230°C while other parameters were fixed (Table 4). Through this various parameter done a set of optimum deposition parameters was obtained; consist of optimum chamber pressure, electrode distance, CH_4 flow rate and substrate temperature.

Table 1 Deposition parameters for different chamber pressure (Set 1)

Sample	Chamber pressure (Torr)	Power (W)
A01	0.1	0.3976
A02	0.2	0.2989
A03	0.4	0.2340
A04	0.6	0.1968
A05	0.8	0.1634

With other parameters fixed at: electrode distance, 2.5 cm, CH_4 flow rate, 5 sccm, substrate temperature, 30°C and deposition time, 5 h

Table 2 Deposition parameters for different electrode distance (Set 2)

Sample	Electrode distance (cm)	Power (W)
A06	1.5	0.3740
A07	2.0	0.3162
A08	2.5	0.2989
A09	3.0	0.1530
A10	3.5	0.1290

With other parameters fixed at: chamber pressure, 0.2 Torr, CH_4 flow rate, 5 sccm, substrate temperature, 30°C and deposition time, 5 h

Table 3 Deposition parameters for different CH_4 flow rate (Set 3)

Sample	CH_4 flow rate (sccm)	Power (W)
A11	1	0.3380
A12	3	0.3150
A13	5	0.2989
A14	7	0.2288
A15	9	0.2016

With other parameters fixed at: chamber pressure, 0.2 Torr, electrode distance, 2.5 cm, substrate temperature, 30°C and deposition time, 5 h

Table 4 Deposition parameters for different substrate temperature (Set 4)

Sample	Substrate temperature (°C)	Power (W)
A16	30	0.3150
A17	80	0.3213
A18	130	0.3328
A19	180	0.3445
A20	230	0.4218

With other parameters fixed at: chamber pressure, 0.2 Torr, electrode distance, 2.5 cm, CH_4 flow rate, 3 sccm and deposition time, 5 h

6 Sample Characterizations

6.1 Structural and Optical Analysis

Infrared and Raman spectroscopy, UV–Visible Spectrophotometer and photoluminescence are normally used to investigate the structural and optical properties of a-C:H thin films.

6.1.1 Infrared Spectroscopy

The infrared spectroscopy characterization of the a-C:H samples was done within the region from 400 to 4,000 cm^{-1}. The basic principle of infrared spectroscopy is the vibrations of the atomic molecule. The sub-molecular groups in the complex molecules structure possess their own natural vibration frequencies, which is generally in the infrared region. During infrared radiation (with broad range of the frequencies) on the sub-molecule, the sub-molecular groups in the molecule absorb the radiation frequencies, which meet their natural frequencies. Accordingly, the specific frequencies or wave numbers at which a molecule absorbs infrared radiation with the structure of the molecule can be feasibly correlated. The hydrogen incorporation into a-C:H films is possibly in the form of CH, CH_2, or CH_3 groups and the carbon to hydrogen bonding maybe sp^3, sp^2, or sp hybridized [10].

During infrared measurement, a bare corning glass substrate was used as a reference to cancel the substrate effects. The resolution of the measurement was 4 cm^{-1} and 100 scans to ensure a good signal to noise ratio. The final infrared spectrum should be free of all the environmental contributions (water vapor and CO_2) the background scanned should be done first.

6.1.2 Laser Raman Spectroscopy

Raman spectroscopy is often said to be complementary to infrared spectroscopy [23]. In Raman measurement, the sample is irradiated by intense laser beam of frequency, v_o, (typically argon (Ar^+) laser wavelength of 514.5 nm) and the scattered light is detected. The scattered lights consist of two types; Rayleigh and Raman scattering. The Rayleigh scattering is an elastic collision between the incident photon and the molecule; therefore the frequency of the scattered photon is the same as that of the incident photon. This is the strongest component of the scattered radiation. Raman scattering is an inelastic collision between the incident photon and the molecule. The signal is very weak and is $\sim 10^{-5}$ of the incident beam which occurs in the range of ultraviolet to infrared region. The Raman spectrum line depends on the emitted photon frequency, the photon that shifts to a lower frequency is known as *Stokes line*. For a higher frequency of emitted photon this is known as an *anti-Stokes line*. This is due to less energetic final vibrational state as compared to the initial state. With the existence of frequency lines, which represents the vibration by certain material bonding, therefore the presence of amorphous structure could be known [23].

During Raman spectra measurement, the spectra of a-C:H films were scanned from 0 to 2,000 cm^{-1}. The spectra were curve-fitted using a program called GRAMS/32. The disorder (D) and graphite (G) peaks were fitted with Gaussian lineshapes on a quadratic baseline, and the substrate peak (if present at 1,095 cm^{-1}) was fitted with a Gaussian lineshape on a linear baseline. Values for the position, intensity, and full width half maximum (FWHM) of the G and D peaks respectively were recorded from the curve fitting.

6.1.3 UV/Visible Spectrophotometer

The main purpose of using UV–Vis spectrophotometer is to estimate the a-C:H thin film optical band gap (E_0). The optical band gap was obtained by the linear extrapolation of the $\sqrt{\alpha h\nu}$ versus photon energy, $h\nu$ graph using the Tauc plot [10]. The transmittance, reflectance, and absorption measurement were performed in a working range of 300–3,000 nm. Two radiation sources were used which is halogen/tungsten lamp for VIS/NIR region (340–2,500 nm) and deuterium lamp for UV region (190–350 nm). The scanning procedure starts by placing bare corning glass substrate in the reference holder and performing base line correction. The base

line operation is to perform background correction over a certain selected wavelength range. Then placed the sample in the sample holder and the transmission scanning was obtained over the selected wavelength.

6.1.4 Photoluminescence Spectroscopy

One of the interesting features of a-C:H is its capability to exhibit strong photoluminescence (PL) emission at room temperature. PL spectroscopy is a technique that uses the photo excitation and recombination of electron-hole pairs to determine the structural and optical properties of the material. The recombination mechanism of a-C:H is affected by the disorder which cause tail state within the gap and by the defect state at mid-gap (dangling bond). This would influence the luminescence intensity. The PL mechanism is an effective tool to extract the information about the nature and the energy state of disordered a-C:H material.

The PL recombination process consists of two consecutive steps as shown in Fig. 2. The electron and hole initially lose their energy by number of transitions as they thermalize into the tail states followed by recombination which can be either radiative or non-radiative. The recombination which involves an emission of photon is designated as radiative recombination process and for non-radiative recombination process it involves emission of phonon which provides other recombination pathway. This does not contribute to the luminescences spectrum [10, 24]. The PL excitations can be achieved using special xenon flash tube, which produces an intense, short duration pulse of radiation over the spectral range of instrument (200–800 nm) to create electron-hole pairs. Pre-scan were done on the sample before an excitation scan.

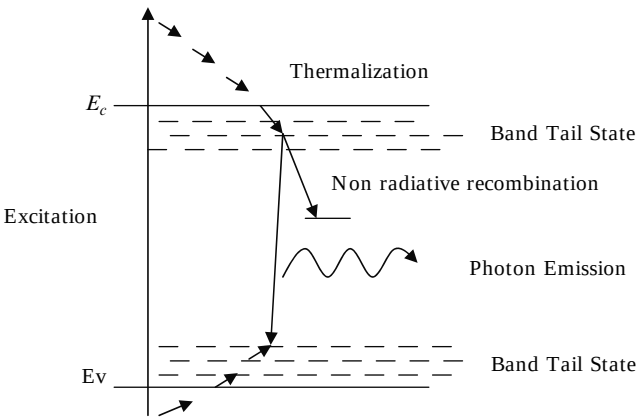

Fig. 2 Thermalization, radiatiave and non-radiative recombinations mechanism occurs in a-C:H structure [10]

6.2 Measurement of Film Thicknesses

Generally, there are several ways of measuring film thicknesses one of them is ellipsometry technique.

6.2.1 Ellipsometer

The basic principle of ellipsometry technique is by radiating the surface of the sample with monochromatic light (with known wavelength and polarity). Then, the polarity of the reflected light was analyzed. Multiple incident angle ϕ was used. Helium-neon laser with wavelength of 632 nm was used as light source. The equipment calibration was done based on standard silicon material by adjusting the analyzer meter and the pole on the ellipsometer equipment. Parameters obtained from the ellipsometer measurement were $A_{1'}$ and $A_{2'}$. Both were reading from the first and second analyzer respectively. Other than that, P_1 and P_2 were the reading from the first and second polarizer respectively. All the data were then entered into the BBC Ellips software in order to determine the thickness of the thin films.

7 Structural and Optical Properties of a-C:H Films

The results and discussions on the structural and optical properties of a-C:H are usually based on analysis from infrared and Raman spectroscopy, UV–Vis Spectrophotometer and photoluminescence.

7.1 Infrared Spectra

The structural characterization of a-C:H films is complicated due to their amorphous nature. The typical infrared spectra of a-C:H is a wide absorption band centered at about 2,900 cm^{-1}. Most of the researchers pay great attention to the C–H stretching band which is observed in the range of 2,800–3,200 cm^{-1}. In this region the complicated absorption bands originated from C–H vibrations with carbon atoms in various hybrid electronic states, such as sp^1, sp^2, sp^3, cyclic and aromatic states of carbon. The sp^1 hybrid is an unusual state in most types of a-C:H films [10]. The interpretation of the absorption peaks are tabulated in Table 5.

The example of infrared spectrum for a-C:H sample prepared by DC-PECVD method at plasma power, w from 0.2989 to 0.4218 W is illustrated in Fig. 3. The strongest and clearest absorption peaks were detected at 2,958, 2,932, 2,872 cm^{-1} which correspond to sp^3 CH_3 (asymmetric), sp^3 CH_2 (asymmetric) or sp^3 CH, and sp^3 CH_3 (symmetric) stretches respectively. From the spectrum, it can be concluded

Table 5 C–H stretch absorption bands for a-C:H

Wave number	Configuration	Olefinic or aromatic	Symmetric (S) or antisymmetric (A)
3,300–3,305	sp^1CH		
3,085	sp^2 CH_2	Olefenic	A
3,035–3,060	sp^2 CH	Aromatic	
3,020–3,025	sp^2 CH_2	Olefenic	
2,990–3,000	sp^2 CH	Olefenic	S
2,960–2,970	Sp^3 CH_3		A
2,975	sp^2 CH_2	Olefenic	S
2,955–2,962	sp^3 CH_3		A
2,920–2,925	sp^3 CH_2		A
2,920–2,925	sp^3 CH		
2,868–2,885	sp^3 CH_3		S
2,850–2,855	sp^3 CH_2		S

From Manage [10], Mutsukura et al. [13], Couderc et al. [25], Thomsen and Reich [26] and etc.

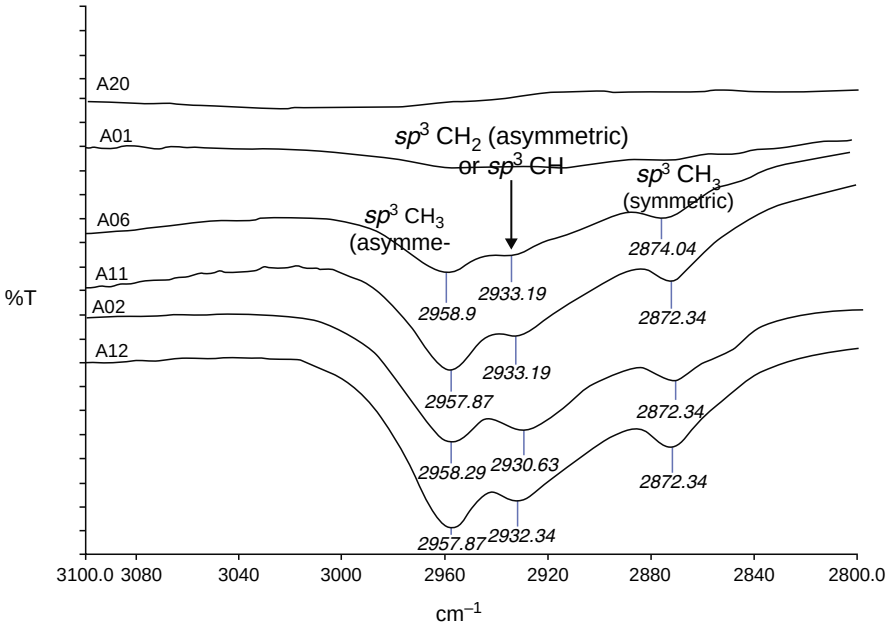

Fig. 3 Typical infrared absorption peak of C–H stretching vibrations of a-C:H thin films deposited at power; 0.2989–0.4218 W by DC-PECVD method

that higher plasma power causes an increase in ion energy, E, which easily breaks C–H bond. This led to the reduction of hydrogen content in the films, increased the sp^2 graphitic behaviour as detected at samples A20 and A01 [21, 27, 28]. As a result of higher plasma power consumption during deposition the films move from polymer to graphite like structure.

7.2 Raman Spectra

The Raman spectra of a-C:H films were dominated by the graphitic carbon features, the graphite (G) and disorder graphite (D) peaks at ~1,580 cm^{-1} and ~1,350 cm^{-1} respectively. Table 6 presents the interpretation of typical Raman features of a-C:H films according to Schwan et al. [29] Tamor and Vassell [30]. The G mode is a bond-stretching vibration of sp^2 sites that is arranged in olefinic chains or aromatic rings. The D mode is the vibrations of a six-membered aromatic ring, which is disorder active. It is only activated when sp^2 sites are in aromatic rings [29, 30].

For an entirely sp^3 bonded a-C material and pure crystalline graphite there is no D peak detected in Raman spectrum. In between these properties there is a ratio of G & D intensity peak (I_D/ I_G) [31], that is dependent on the size of graphitic clusters [32]. The I_D/I_G ratio can be correlated with qualitative information of sp^3/sp^2 ratio in the films. The increase of the I_D/I_G ratio indicates a higher disorder of a-C:H films and the decrease of the ratio of sp^3 content to sp^2-bonded carbon configuration [26, 33].

According to Ferrari and Robertson [34] the Raman spectrum of a film depends on four factors:

1. The clustering of the sp^2 phase
2. The extent of bond disorder
3. The presence of sp^2 rings or chains
4. The sp^2/sp^3 ratio

The positions, widths, and relative intensities of the D and G peaks are found to vary systematically with deposition parameters. The example of Raman spectrum of a-C:H films deposited by DC-PECVD method at power, *w* between 0.2989 and 0.4218 W is shown in Fig. 4. The details of the spectral were tabulated in Table 7. From the spectrum, it can be seen that plasma power affected the G and D peaks position, width, I_D/I_G ratio and curve background slope. The higher the power, the greater the G and D peaks shifted and I_D/I_G ratio increases as well. The higher power also causes the G peak to become narrower and background slope to reduce. This suggested that the films deposited at high power have high sp^2 content and larger cluster size compared with films deposited at low power.

Table 6 Positions and interpretation of Raman peaks [29, 30]

Peak	Wave number (cm^{-1})	Interpretation
D	~1,350	Microcrystalline mode of graphite sp^2 stretch vibration in aromatic ring which is activated by disorder
G	~1,580	Center vibration mode of graphite sp^2 stretch vibration of olefinic chains sp^2 stretch vibration in aromatic or condensed aromatic rings

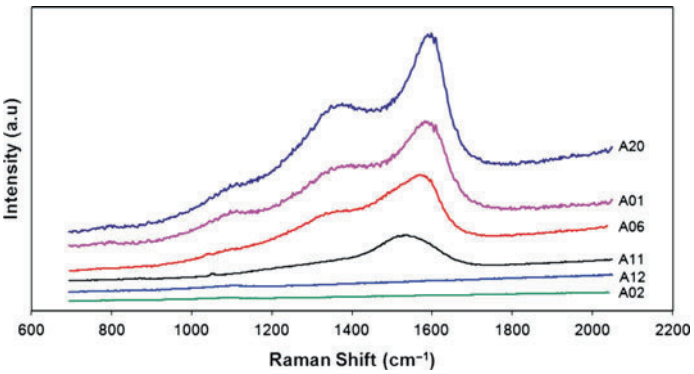

Fig. 4 Raman spectrum of a-C:H thin films deposited at various DC powers 0.2989–0.4218 W

Table 7 The position and width of G and D peaks, the slope value and I_D/I_G ratio of a-C:H in the 1,300–1,600 cm^{-1} range

Samples	D.C power, *w*	G-peak (cm^{-1})	G-width	Slope	D-peak (cm^{-1})	D-width	I_D/I_G Ratio
A20	0.4218	1,598	92.53	1.45	1,361	343.90	0.88
A01	0.3976	1,588	111.21	1.73	1,356	386.25	0.76
A06	0.3740	1,576	128.43	2.56	1,340	425.10	0.66
A11	0.3380	1,540	157.73	3.12	1,335	448.04	0.42
A12	0.3150	0	0	6.73	0	0	0
A02	0.2989	0	0	6.84	0	0	0

7.3 *Optical Band Gap*

The optical properties of a-C:H thin films have been extensively studied by many researchers with various forms of deposition technique. Table 8 show the correlation of film properties and deposition parameter on optical band gap, E_o. The E_o value can be tuned by adjusting the deposition parameter, as for higher E_o value the trend of deposition parameter such as substrate temperature, chamber pressure and etc. must be reduced to an optimum value. The reverse result; low E_o can be obtained by reversing deposition parameter to an increase value.

In order to determine the optical transition in a-C:H thin films, graphs of $(\alpha h\upsilon)^2$, $(\alpha h\upsilon)^{2/3}$, $(\alpha h\upsilon)^{1/2}$, $(\alpha h\upsilon)^{1/3}$ have been plotted versus photon energy, $h\upsilon$. Graphs of $(\alpha h\upsilon)^2$ and $(\alpha h\upsilon)^{2/3}$ versus photon energy determines the allowable and forbidden direct transition, respectively. Meanwhile, graphs of $(\alpha h\upsilon)^{1/2}$ and $(\alpha h\upsilon)^{1/3}$ versus photon energy shows the allowable and forbidden indirect transition. Optical band gap, E_0 can be gained by extrapolating the linear section of the curves until it crosses the x-axis (photon energy). The value at the intersection point on the x-axis is the optical band gap, E_0. Figure 5 shows the example of allowable indirect

Table 8 The correlation of film properties and deposition parameter on optical band gap, *E*

Film-property	Deposition parameter	E_os value	Reasons	Deposition technique
H content increase (polymer like a-C:H, soft film, in some study show low refractive index, *n*, value)	Power, *w*, substrate temperature, negative bias voltage, chamber pressure, – were all reduced	Increase	Increases in sp^3 content/ reduction of sp^2 content	DC saddle field glow discharge [10, 18] RF-PECVD [35–37] DC-PECVD [38] ECR-RF PECVD [39]
sp^2 content increase (graphite like structure, higher hardness, and *n* value)	Power, *w*, substrate temperature, negative bias voltage, chamber pressure, – were all increased	Decrease	Increment in graphitic cluster size and chain length	DC saddle field glow discharge [10, 18] ECR-microwave CVD [20] RF-PECVD [35–37] DC-PECVD [38]

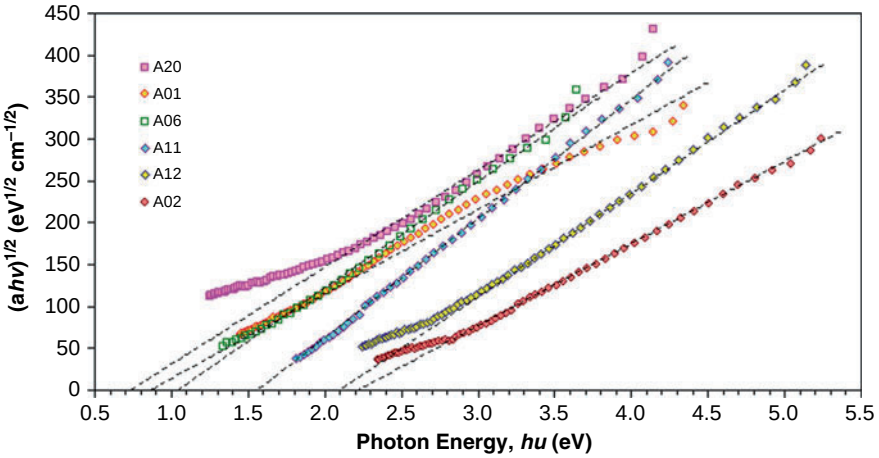

Fig. 5 Graph of $(\alpha h\upsilon)^{1/2}$ vs photon energy, $h\upsilon$ of a-C:H thin films at various DC powers 0.2989–0.4218 W

transition, $(\alpha h\upsilon)^{1/2}$ as a function of photon energy, $h\upsilon$ graph. The values of optical band gap of a-C:H thin films from DC-PECVD method for all type of optical transition are listed in Table 9. Generally, the table shows that the optical band gap values decreased with the increase of power from 0.2989 to 0.4218 W. It can be said that the decreased in sp^3 CH_3 bonding occurred in a-C:H films upon the increase of power during the deposition, led the decreased in the optical band gap. It was found that the E_0 value decreases when the sp^2 fraction in the films increased with increasing power and this was vice-versa for lower power value. This is also

Table 9 Values of optical band gap of a-C:H thin film at the respective DC power

Sample	DC power (W)	Optical band gap, E_0 (eV)			
		Allowable direct transition	Forbidden direct transition	Allowable indirect transition	Forbidden indirect transition
A02	0.2989	3.51	2.41	2.22	1.45
A12	0.3150	3.37	2.22	2.11	1.19
A11	0.3380	2.83	1.98	1.58	0.88
A06	0.3740	2.65	1.29	1.05	0.03
A01	0.3976	2.20	1.48	0.88	0.31
A20	0.4218	2.05	1.11	0.75	0.00

consistent with Robertson model [6]. According to this model, amorphous carbon consists of sp^2 clusters which were embedded in the sp^3 bonded matrix. Since sp^2 clusters form band edges, therefore they control the band gap. Bigger sp^2 clusters have lower E_0, while smaller sp^2 clusters have larger E_0 value.

7.4 Photoluminescence

A very broad photoluminescence (PL) spectra which cover entire visible range, centered at 2.1–2.3 eV have been reported by numerous study for a-C:H films. According to Rusli et al. [40], the PL intensity spectra could be associated as the number of dangling bonds in the films. The decreased in the PL intensity indicates high dangling bond concentration as less hydrogen attached to carbon atoms to terminate the bonds. For the relation between PL peak energy and optical gap shows that as optical gap decreases, the red shift of PL peaks occurs, however there was no clear relationship between them observed [41]. The photoluminescence (PL) data which was obtained from the a-C:H sample prepared at different power, w from 0.2989 to 0.4218 W using DC-PECVD is shown in Fig. 6. Here one can find that there were significant changes in the PL intensity and a slight peak shifting between them. As the structure in a-C:H films moves from a polymer-like (low power) to a graphite-like structure (high power), the PL intensity decreases. This was accompanied by a red shift of the PL peak energy, as the peak shifted from 1.93 to 1.42 eV. From the analysis, sample A02 showed highest PL peak energy value at 1.93 eV, containing smaller sp^2 cluster size compared with other samples.

The films which exhibit strong photoluminescence were the soft a-C:H films which have higher hydrogen concentration and greater optical band gaps. The red shift can also be explained by the increased in cluster size with the increasing power hence ion energy during deposition [10, 14, 40]. As the ion energy increases, the sp^2 cluster size in a-C:H increases, resulting in smaller optical band gaps, and finally, shift the photoluminescence peak energy towards lower energy.

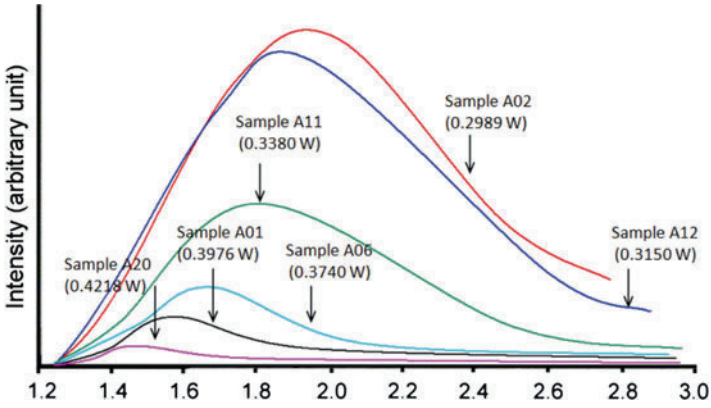

Fig. 6 The photoluminescence spectrum for a-C:H films deposited at various DC powers 0.2989–0.4218 W

8 Ions Bombardment Calculation

Ions play a crucial role in the growth mechanism of a-C:H thin film. Ions can create dangling bond sites on the film surface which are more likely causes the radicals to bond on the film surface through the dangling bond sites [10]. Therefore, the adsorption rate of the radicals on the surface is strongly dependent on the dangling bond generation rate [10, 13]. The generation of dangling bond depends on the energy and the flux of ions reaching the substrate. The major ionic species in the CH_4 plasma are the CH_3^+ ions [10]. The energy of CH_3^+ ions reaching the substrate increases with increasing power, w. The number of radicals which participate in the growth increases as well, with increasing power.

Hence the calculation of the ion bombardment was done as follow:
The ion bombardment, E is described as [6]:

$$E \sim V\left(\frac{\lambda_{mfp}}{L}\right) \tag{1}$$

where λ_{mfp} is the mean free path (mfp) of the particles within the ion sheath,

$$\lambda = \frac{kT}{\sqrt{2}p\sigma} \tag{2}$$

and k is the Boltzmann constant (1.38066×10^{-23} J K^{-1}). T is the plasma temperature in Kelvin (K). We assume that plasma temperature is somewhat above ambient since the electron and ion temperature is very high ~23,200 K and 500 K, respectively, while the neutral temperature is low ~293 K so the estimated

value of plasma temperature is ~400 K. The plasma temperature will be higher than that if the substrate temperature is higher, ~500 K [42]. p is the pressure in Pascal and σ is the collision cross-section of CH_3^+ ions (~100 Å^2). We assume that the cross-section of CH_3^+ ions with the CH_4 molecules should be higher than CH_4 molecules with CH_4 molecules (since the cross-section of CH_4 is ~46 Å^2). Where L is the thickness of the ion sheath within DC glow discharge given by May [43] from the modified version of Morgan's equation [44]

$$L_{\max} = 2.12 \times 10^{-5} \left\{ {}^1\!/\!_2 e / \left(3.5 \times 10^{19} p m_i \sigma\right) \right\}^{1/5} (V_{\max})^{3/5} \tag{3}$$

and p is the pressure, m_i is the mass of the major ionic species, σ and $V_{\max}$ are the collision cross-section of CH_3^+ and sheath potential. Here we assume that the voltage, V which is being measured is equal to sheath potential with plasma potential, V_p neglected since it is usually only around 10–30 V in the DC glow discharge [42]. For $p = 0.1$–0.2 Torr, $V = 490$–570 V we find that, $\lambda = 0.148$–0.294 mm and $L = 4.45$–5.54 mm. Figure 7 shows an example plot of the sheath thickness against pressure and the line shows the value of sheath thickness at $p = 200$ mTorr for the sample A20. The sheath thicknesses which were obtained are consistent with visual observations during the experiment, which is about a couple of millimeter.

Figure 8 shows a plot of ion bombardment energy, E against power, w. Generally, it can be seen that E increases from 16.26 to 29.67 eV with increasing power, w from 0.2989 to 0.4218 W. It was found that sample A01 showed the highest E value which was 29.67 eV and sample A02 showed the lowest E value which was 16.26 eV. Rather than ion bombardment energy which contributes to the removal of hydrogen from the surface, the hot substrate (230°C) is also capable of removing the hydrogen by thermal evaporation. Since the hydrogen is low mass and the C–H bonding energy, E_B is low ~4 eV, compared to –C–C– (15.6 eV) the hydrogen will be preferentially evaporated [45].

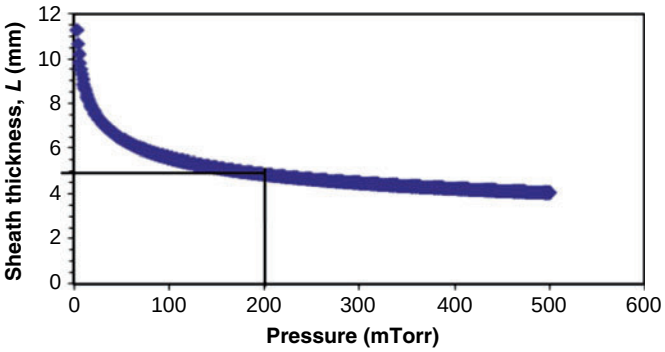

Fig. 7 A plot of the sheath thickness against pressure and the dashed line shows the value of sheath thickness at $p = 200$ mTorr for sample A20

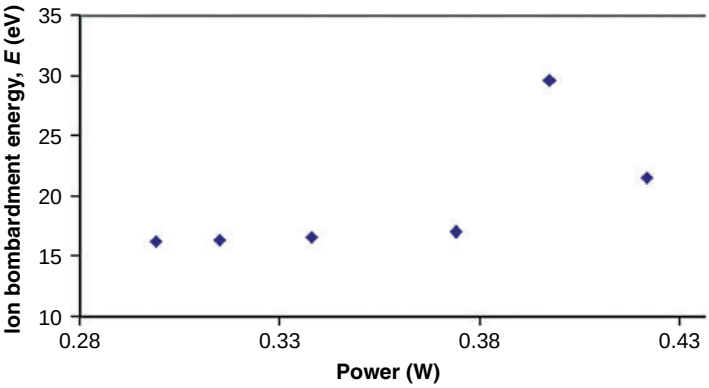

Fig. 8 A plot of ion bombardment energy, E of a-C:H thin films at different powers, w

The ion bombardment can causes the hydrogen to sputter from the surface [10, 36]. High energy ions can penetrate deeper into the growing film, compared to the low energy during the deposition. More hydrogen atoms were removed both from the surface and the subsurface atomics layers of the growing film. As a result, the H/C ratio in the film decreases with increasing ion energy. More sp^2 bonds and bigger clusters were formed as the ions energy increases. As for low energy ion, the removal of hydrogen from the growing films and creation of sp^2 sites were not efficient. The resulting films were soft a-C:H films with a high hydrogen concentration, a high sp^3 fraction (a large number of the sp^3 carbons were in the form of the sp^3 CH_3 configuration), and a low sp^2 fraction with small cluster. Due to the small cluster size, the soft a-C:H films have larger optical band gaps, as E decreased.

9 Conclusion

In this chapter the synthesis of a-C:H films using the DC-PECVD method was discussed in detailed. Experimental results on the effect of deposition parameters such as chamber pressure, electrode distance, CH_4 flow rate, and substrate temperature on the a-C:H structural and optical properties were presented and discussed. Structural and optical properties of a-C:H thin films based on infrared and Raman spectroscopy, UV–Vis spectrophotometry and photoluminescence spectroscopy analyses were presented. The sp^3/sp^2 and hydrogen contents, optical gap, E_0 and photoluminescence properties of a-C:H films were strongly dependent on the plasma power and ion bombardment energy which resulted from varying the deposition parameters. The most interesting feature of a-C:H is its various properties (either diamond or graphite-like structure) which can be done by manipulating the deposition parameter. Hence, each property can be customized for specific applications.

Acknowledgements I would like to express my gratitude to UPSI, MARA, UTM and UiTM for the financial and technical support on this project.

References

1. Chopra, K.L.: Thin Film Device Application. Plenum, New York (1969)
2. Kazmerski, L.L.: Polycrystalline and Amorphous Thin Films and Devices. Academic, New York (1980)
3. Ibrahim Abu Talib, Mustaffa Hj. Abdullah, Sahrim Hj. Ahmad: Sains Bahan, 2nd edn. Dewan Bahasa dan Pustaka, Kuala Lumpur (1993)
4. Dachuan, Y., Niankan, X., Zhengtang, L., Yong, H., Xiulin, Z.: Surf. Coatings Technol. **78**(1–3), 31–36 (1996)
5. Grill, A.: IBM. J. Res. Develop **43**(1/2), 147–160 (1999)
6. Robertson, J.: Mater. Sci. Eng. R **37**, 129–281 (2002)
7. May, P.W.: CVD diamond: a new technology for the future? Elsevier Science Ltd., 10–106 (1995)
8. May, P.W.: Phil. Trans. R. Soc. Lond. A **358**, 473–495 (2000)
9. Smith, J.A.: PhD thesis, University of Bristol, UK (2001)
10. Manage, D.P.: PhD thesis, University of Toronto, Canada (1998)
11. Aisenberg, S., Chabot, R.: J. Appl. Phys **42**(7), 2953–2958 (1971)
12. Angus, J.C.: Thin Solid Films **142**(1), 145–151 (1986)
13. Mutsukura, N., Inoue, S., Machi, Y.: J. Appl. Phys **72**(1), 43–53 (1992)
14. Rusli, Amaratunga, G.A.J., Silva, S.R.P.: Opt. Mater. **6**, 93–98 (1996)
15. Jing, Q.C.: PhD thesis, University of Texas at Dallas, US (1999)
16. Bouree, J.E., Godet, C., Etemadi, R., Drevillon, B.: Synth Met **76**, 191–194 (1996)
17. Taube, K.: Surf. Coatings Technol. **98**(1–3), 976–984 (1998)
18. Sagnes, E.: PhD thesis, University of Toronto, Canada (1998)
19. Cheng, Y.H., Wu, Y.P., Chen, J.G., Qiao, X.L., Xie, C.S., Tay, B.K., Lau, S.P., Shi, X.: Surf. Coatings Technol. **135**(1), 27–33 (2000)
20. Zhou, X.T., Lee, S.T., Bello, I., Cheung, A.C., Chiu, D.S., Lam, Y.W., Lee, C.S., Leung, K. M., He, X.M.: Mater. Sci. Eng. B **77**, 229–234 (2000)
21. Hong, J., Goullet, A., Turban, G.: Thin Solid Films **364**(1–2), 144–149 (2000)
22. Hong, J., Lee, S., Cardinaud, C., Turban, G.: J. Noncrystalline Solids **265**(1–2), 125–132 (2000)
23. Long, D.A.: Raman Spectroscopy. McGraw-Hill, London (1977)
24. Morigaki, K.: Physics of Amorphous Semiconductor. Imperial College Press, London (1999)
25. Couderc, P., Catherine, Y.: Thin Solid Films **146**(1), 93–107 (1987)
26. Thomsen, C., Reich, S.: Phys. Rev. Lett. **85**, 5214 (2000)
27. Cho, Y.O., Cho, J.M., Jun, W.J., Cha, O.H., Suh, E.K., Yu, K.H., Yu, S.C., Lee, J.K.: Diam. Relat. Mater. **11**(11), 1848–185 (2002)
28. Lacerda, R.G., Tojolan, V.S., Cox, D.C., Silva, S.R.P., Marques, F.C.: Diam. Relat. Mater. **11** (3–6), 990–984 (2002)
29. Schwan, J., Ulrich, S., Ehrhardt, H., Silva, S.R.P.: J. Appl. Phys. **80**(1), 440–447 (1996)
30. Tamor, M.A., Vassell, W.C.: J. Appl. Phys. **76**(6), 3823–3830 (1994)
31. Kleinsorge, B., Rodil, S.E., Adamopoulos, G., Robertson, J., Grambole, D., Fukarek, W.: Diam. Relat. Mater. **10**(3–7), 965–969 (2001)
32. Tuinstra, .F, Koenig, J.: J. Chem. Phys. **53**, 1126 (1970) in Schwan, J., Ulrich, S., Ehrhardt, H., Silva, S.R.P.: J. Appl. Phys. **80**(1), 440–447 (1996)
33. Lejeune, M., Durand-Drouhin, O., Henocque, J., Bouzerar, R., Zeinert, A., Benlahsen, M.: Thin Solid Films **389**(1–2), 233–238 (2001)

34. Ferrari, A.C., Robertson, J.: Interpretation of Raman spectra of disordered and amorphous carbon. Phys. Rev. B. **61**(20), 14095–14107 (2000)
35. Filik, J., May, P.W., Pearce, S.R.J., Wild, R.K., Hallam, K.R.: Diam. Relat. Mater. **12**(3–7), 974–978 (2003)
36. Budenzer, A., Dischler, B., Brandt, G., Koidl, P.: J. Appl. Phys **54**(8), 4590–4595 (1983)
37. Serra, C., Pascual, E., Maass, F., Esteve, J.: Surf. Coatings Technol. **47**(1–3), 89–97 (1991)
38. Suriani, A.B.: MSc thesis, Universiti Teknologi Malaysia, Malaysia (2005)
39. Durand-Drouhin, O., Zeinert, A., Benlahsen, M., Zellama, K., Kre, R., Turban, G., Grosman, A.: Diam. Relat. Mater **9**(3–6), 752–755 (2000)
40. Rusli, Amaratunga, G.A.J., Silva, S.R.P.: Thin Solid Films **270**(1–2), 160–164 (1995)
41. Demichelis, F., Tagliaferro, A., Gupta, D.D.: Surf. Coatings Technol. **47**(1–3), 218–223 (1991)
42. Chapman, B.: Glow Discharge Processes. Wiley-Interscience, New York (1980)
43. May, P.W.: PhD thesis, University of Bristol, UK (1991)
44. Morgan, R.A., PhD thesis, University of Sussex, UK (1985)
45. Craig, S., Harding, G.L.: Thin Solid Films **97**(4), 345–361 (1982)